PCCP

Accepted Manuscript

ROYAL SOCIETY OF CHEMISTRY

www.rsc.org/pccp

Physical Chemistry Chemical Physics
CREATED USING THE RSC LaTeX PCCP ARTICLE TEMPLATE – SEE www.rsc.org/electronicfiles FOR DETAILS
ARTICLE TYPE www. rsc.org/xxxxxx | XXXXXXXX

Mechanisms of Fluorescence Decays of Colloidal CdSe-CdS/ZnS Quantum Dot Unraveled by Time-Resolved Fluorescence Measurement

Hao Xu, Volodymyr Chmyrov, Jerker Widengren, Hjalmar Brismar, and Ying Fu*

Received Xth XXXXXXXXXX 20XX, Accepted Xth XXXXXXXXX 20XX
First published on the web Xth XXXXXXXXXX 200X
DOI: 10.1039/b000000x

By narrowing the detection bandpass and increasing the signal-to-noise ratio in measuring time-resolved fluorescence decay spectrum of colloidal CdSe-CdS/ZnS quantum dot (QD), we show that directly after the photoexcitation, the fluorescence decay spectrum is characterized by a single exponential decay, which represents the energy relaxation of the photogenerated exciton from its initial high-energy state to the ground exciton state. Fluorescence decay spectrum of long decay time is in the form of β/t^2, where β is the radiative recombination time of the ground-state exciton and t is the decay time. Our findings provide us with a direct and quantitative link between fluorescence decay measurement data and fundamental photophysics of QD exciton, thereafter a novel highway of applying colloidal QDs to study microscopic physical and chemical processes in many fields including biomedicine.

1 Introduction

Colloidal quantum dots (QDs) have been extensively studied[1–4], developed[5–8] and utilized for many applications including in biomedical fields[9–11] and optoelectronics field[12–15]. Extensive reviews about various aspects of QDs can be found readily in literature such as Ref.[16–19]. Though fundamental photophysics behind the superb and unique optical properties of these QDs is well understood, quantitative match between theory and experiment is limited. One major issue is about time-resolved fluorescence decay spectrum. A picosecond laser pulse is led into a QD ensemble[2,8,20–22], even to a single QD[1], and the QD fluorescence is detected as a function of time, denoted as $F(t)$, i.e., the aforementioned time-resolved fluorescence decay spectrum. Multi-exponential model is commonly used to fit $F(t)$, and the number of exponential decay terms varies widely in literature[5,8,14,21,23–27]. In Ref.[27], Nadeau et al. used the one-state trapping model with three fitting parameters to fit the fluorescence decay spectra of mercaptopropionic acid (MPA) coated CdTe QDs under the influence of β-mercaptoethanol (BME), while the fitted data did not display clear relationships with the changes (pH value and BME concentration) in the QD solutions (note that the stretched model and two-exponential model were also used for comparison). It was reported recently[4] that $F(t)$ was well described by the standard bi-exponential model

$$F(t) = F_0 + A_1 \exp\left(-\frac{t-t_0}{\tau_1}\right) + A_2 \exp\left(-\frac{t-t_0}{\tau_2}\right) \quad (1)$$

both numerically (fitting convergence) and physically (the physical parameters in the above expression showed clear trends following the change in the QD environment). For 3-MPA coated CdSe-CdS/ZnS QDs dispersed in 4-(2-hydroxyethyl)-1-piperazineethanesulfonic acid (HEPES) buffer containing 50 mM HEPES and 23 mM NaOH with a pH value of 7.2, $\tau_1 \approx 14$ ns while $\tau_2 \approx 2$ ns, both of them decreased when Ca^{2+} ions were added to the QD solution then recovered when Ca^{2+} ions were removed[4].

Another fundamental issue is about the broad QD fluorescence peak. The full width at half maximum (FWHM) of the QD fluorescence peak is reported to be about 25 nm[28–30]. In aqueous solution this value is usually much larger. Such a broad peak is commonly attributed to the distribution of QD sizes in the QD solution[14,31]. A simple estimation using published formulae[32] showed that the large FWHM could be attributed to a distribution δr in QD radius r of $\delta r/r \approx \pm 10\%$, in agreement with high-resolution transmission electron microscopy (HRTEM) imaging[14]. On the other hand, the measured FWHM of single QDs was shown to be similar to the FWHM of a QD ensemble[33], implying additional factor(s) in understanding the large FWHM of single QDs. Furthermore, a quantum Monte Carlo simulation of single QD fluorescence resulted in also a large FWHM when resonance and off-resonance radiative recombination processes of the

Science for Life Laboratory, Department of Applied Physics, Royal Institute of Technology, SE-106 91 Stockholm, Sweden; E-mail: fu@kth.se

ground-state exciton, i.e., the broadening of the fluorescence peak from time-dependent Golden rule, were included in the simulation[32,34].

In this work we study quantitatively time-resolved fluorescence decay spectrum of water-soluble 3-MPA coated CdSe-based QDs as a function of the detection bandpass, detection wavelength, and integration time in order to unravel the principal QD fluorescence decay processes and to explore the origins of the large FWHM of colloidal QDs.

2 Time-resolved fluorescence measurement

We focus on water-soluble CdSe-CdS/$Cd_{0.5}Zn_{0.5}S$/ZnS core-multishell QDs fabricated in-house using common recipes[4]. Standard structure characterizations including core, shell, QD size distribution and surface ligands of these QDs have been performed, and details were published, see, e.g., Ref.[14,35]. Consisting of a CdSe core, a CdS shell of 2 monolayers, another shell of 1 monolayer $Cd_{0.5}Zn_{0.5}S$, and 1.5 monolayer ZnS, these QDs were coated with 3-MPA surface ligands and had a fluorescence peak at 596 nm at room temperature. They were dispersed in HEPES buffer. These QDs were isolated single QDs confirmed experimentally by dropping 10 μL QD solution on a microscope slide then imaging using an AxioObserver.D1 microscope (Carl Zeiss) showing characteristic single QD blinking. All experimental measurements were performed at room temperature.

Electron energy levels in a QD is characterized by quantized exciton levels[36–38]: The valence-band sublevels in an as-grown QD are completely filled and the conduction-band sublevels are completely empty, which is denoted as the vacuum state ψ_0; One electron initially occupying a valence-band sublevel transits to an empty conduction-band sublevel after absorbing a photon, leaving a hole in the valence-band sublevel. The electron and hole interact with each other via their Coulombic interaction to form an exciton which is enforced by the spatial confinement of the nano-size QD. Since the excitation photon normally is high in energy, the photogenerated exciton is in an excited exciton state ψ_n. The excited exciton relaxes to the ground exciton state ψ_1 via nonradiative interactions, then radiatively recombine to emit a photon, i.e., fluoresce, after which the QD returns to its vacuum state ψ_0.

The time-dependent wave function of the quantum state of the QD is

$$\sum_k C_k(t)\psi_k$$

where k runs over all exciton states. Writing the interaction potential s for either non-radiative energy relaxation or radiative photon emission as

$$V_s'^{+} b_s e^{-i\omega_s t} + V_s' b_s^{+} e^{i\omega_s t} \qquad (2)$$

where b_s^{+} and b_s are the creation and annihilation operators, and $\hbar\omega_s$ is the energy of the interaction such as a phonon (non-radiative energy relaxation) or a photon. Denoting the number of phonons or photons as N_s, the following equations for quantum state coefficients are obtained from time-dependent Schrödinger equation

$$i\hbar\frac{dC_q(t)}{dt} = \sum_k C_k(t)\left[\langle q|V_s'^{+}|k\rangle e^{i(E_q-E_k-\hbar\omega_s)t/\hbar}\sqrt{N_s} + \langle q|V_s'|k\rangle e^{i(E_q-E_k+\hbar\omega_s)t/\hbar}\sqrt{N_s+1}\right] \qquad (3)$$

where E_k is the energy of state ψ_k. The first term on the right side of the equation describes the electron transition from state k to q accompanied by absorbing a phonon or a photon, i.e., $E_k+\hbar\omega_s \rightarrow E_q$, while the second term is about emitting a phonon or a photon, $E_k-\hbar\omega_s \rightarrow E_q$.

The probability that the QD emits a photon at time t is proportional to

$$|\langle\psi_0|V_{\text{photon}}|\psi_1\rangle|^2|C_1(t)|^2\left[1-|C_0(t)|^2\right] \qquad (4)$$

For the radiative recombination, s represents the photon field, while the photoexcited exciton ψ_n normally undergoes many nonradiative energy relaxation processes through many other excited exciton states such as electron-phonon interactions in the QD semiconductor material and many transitions to and from surface states on the large superficial surface area of the colloidal QD before it reaches ψ_1. Therefore, the solution of Eq. (3) requires the knowledge of the interaction potentials. More critically, it also needs to involve a large number of excited exciton states in order to obtain a full quantum mechanical description.

In order to quantitatively correlate the principal decay processes to the time-resolved fluorescence decay spectrum, we study the transition rates of the energy relaxation and radiative recombination of an exciton by the following principal decay processes:

1. Three principal exciton levels: Excited exciton state ψ_n (energy E_n), with its occupation $n_n = |C_n|^2$; Ground exciton state ψ_1 (E_1) with occupation $n_1 = |C_1|^2$; Vacuum state ψ_0 (E_0) with occupation $n_0 = |C_0|^2$.
2. Optical excitation to generate an exciton from vacuum to ψ_n.
3. ψ_n-exciton relaxes at a rate $1/\tau$ to ψ_1 nonradiatively.
4. Ground-state exciton transits radiatively to ψ_0 at a rate $1/\beta$.

In the electron-hole picture, the photoexcitation of the QD is such that an electron originally occupying a valence band sublevel in the QD absorbs a photon to transit to an initially empty sublevel in the conduction band, leaving the valence band

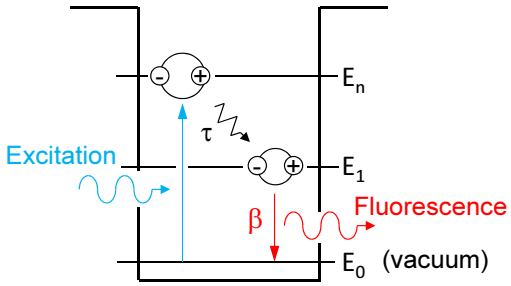

Fig. 1 Schematics of photogeneration, energy relaxation τ and radiative recombination β of an exciton in the QD.

sublevel empty (a hole). The electron in the conduction band sublevel and the hole in the valence band sublevel interact with each other via Coulomb interaction to form an electron-hole pair (i.e., exciton). The electron will relax to the ground sublevel in the conduction band, while the hole will relax to the ground sublevel in the valence band, forming the exciton ground state. The electron at the conduction-band ground sublevel transits to the empty valence-band ground sublevel (i.e., the hole at the valence-band ground sublevel) to emit a photon (QD fluorescence), for which the conduction band sublevels are all empty and the valence band sublevels are all occupied. In other words, the QD returns to its vacuum state.

Following fluorescence decay experimental procedure, the QD is initially at its vacuum state. One pulsed excitation excites the QD at $t = 0$ so that $n_n = 1$ and $n_1 = n_0 = 0$. The decay processes, schematically shown in Fig. 1, are described mathematically by the following rate equations:

$$\begin{aligned} \frac{\mathrm{d}n_n}{\mathrm{d}t} &= -\frac{n_n(1-n_1)}{\tau} \\ \frac{\mathrm{d}n_1}{\mathrm{d}t} &= \frac{n_n(1-n_1)}{\tau} - \frac{n_1(1-n_0)}{\beta} \\ \frac{\mathrm{d}n_0}{\mathrm{d}t} &= \frac{n_1(1-n_0)}{\beta} \end{aligned} \tag{5}$$

which have been commonly applied to study multi-level multi-electron systems, see, e.g., Ref.[39,40]. The key factor here is the Pauli exclusion principle (Fermion anticommutation relations of the electron creation and annihilation operators) that the occupation of one exciton level reduces the efficiencies of transitions to this exciton level since each exciton level can be occupied by only one exciton. As a consequence, the transition efficiency of an exciton from an initial exciton level to a final exciton level is determined by both the occupation of the initial level and the un-occupation of the final level[40].

We performed a numerical simulation of Eqs. (5) using $\tau = 8.0$ ns and $\beta = 2.0$ ns (see more discussions about values of τ and β below). Temporal developments of n_n, n_1, n_0, and the

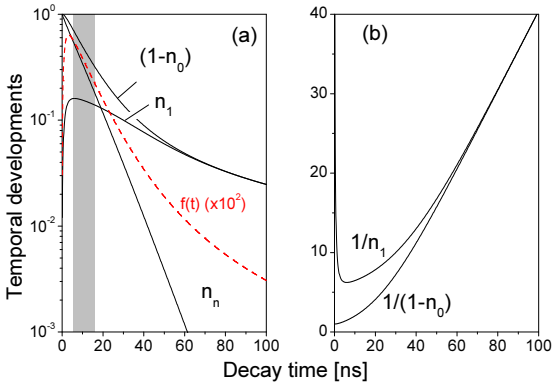

Fig. 2 (a) Temporal developments of n_n, n_1, $(1-n_0)$, and theoretical time-resolved fluorescence decay spectrum $f(t)$ (red line, magnified by 10^2). $\tau = 8.0$ ns, $\beta = 2.0$ ns. (b) $1/n_1$ and $1/(1-n_0)$. $\delta = 0.1$ ns

theoretical time-resolved fluorescence decay spectrum

$$f(t)|_{t=\ell\delta} = \int_{(\ell-1)\delta}^{\ell\delta} \frac{n_1(1-n_0)}{\beta}\,\mathrm{d}t \tag{6}$$

are presented in Fig. 2(a) in a logarithmic scale. Here we tried to simulate the measurement procedure that δ is the integration time of time-to-amplitude-converter (TAC) channels (see below). We observe two distinct decay characters in $f(t)$, a rather fast decay directly after the optical excitation and a slow decay when t is long.

In a very short time directly after the optical excitation, see the shadow area in Fig. 2(a), $f_1(t)$ was well characterized by a single decay term

$$f_1(t) \propto e^{-t/\tau'} \tag{7}$$

for $t \in (5, 15)$. Subscript "1" in $f_1(t)$ indicates the fluorescence decay spectrum of short t. Note that τ' depends on both τ and β, especially when the orders of τ and β are close to each other. In the case of $f(t)$ presented in Fig. 2(a) ($\tau = 8.0$ and $\beta = 2.0$ ns), $\tau' = 11.10$ ns.

A close examination shows that the time-resolved fluorescence character for $t > 60$ ns is very different from the exponential decay of $f_1(t)$. For $t > 60$ ns, Fig. 2(a) shows that n_n is negligibly small so Eqs. (5) reduced to

$$\frac{\mathrm{d}n_1}{\mathrm{d}t} = -\frac{n_1(1-n_0)}{\beta}\ ,\ \ \frac{\mathrm{d}n_0}{\mathrm{d}t} = \frac{n_1(1-n_0)}{\beta} \tag{8}$$

Let $1-n_0 = n_0'$ and $n_1 = n_0'$, the solution of the above equations is

$$\frac{1}{n_1} = \frac{1}{n_0'} = \frac{t+a}{\beta} \tag{9}$$

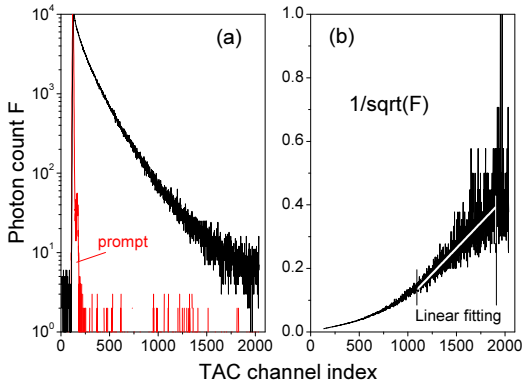

Fig. 3 (a) Time-resolved fluorescence decay spectrum $F(\ell)$ as a function of the time-to-amplitude-converter channel (TAC) index ℓ. (b) $\sqrt{1/F(\ell)}$ and a linear fitting in the TAC channel range of $\ell \in (1100, 1900)$. $\delta = 0.1148971$ ns and $t = \ell\delta$ is the decay time.

where a is a constant. The above solution is confirmed by the numerical results of $1/n_1$ and $1/(1-n_0)$ presented in Fig. 2(b). The long-time fluorescence decay for $t > 60$ ns is thus

$$f_2(t)|_{t=\ell\delta} = \int_{(\ell-1)\delta}^{\ell\delta} \frac{n_1(1-n_0)}{\beta}\,\mathrm{d}t \approx \frac{\beta\delta}{(t+a)^2}\bigg|_{t=\ell\delta} \qquad (10)$$

since the variations of n_1 and $(1-n_0)$ in t is very small in the time duration $\in \Big((\ell-1)\delta, \ell\delta\Big)$. The above expression is hardly exponential and needs many exponential decay terms in order to fit it numerically.

By re-examining all our previously reported time-resolved fluorescence decay spectra $F(\ell)$ such as in Ref.[4,41], we indeed found out that the long-time fluorescence decay spectra matched perfectly with $f_2(t)$ in Eq. (10) by plotting $\sqrt{1/F(\ell)}$ vs. ℓ which was linear in ℓ in a certain range of ℓ, where $F(\ell)$ is the measured time-resolved fluorescence decay spectrum as a function of TAC channel index ℓ. A typical result is shown in Fig. 3. However, the results were not totally unambiguous due to the low signal-to-noise ratios when ℓ was large.

We performed new time-resolved fluorescence measurements of our QDs in the following manner by using a time-correlated single-photon counting machine (FluoroMax-3, Horiba Jobin Yvon). A spectral line centered at 495 nm with a 2 nm bandpass from a pulsed light-emitting diode (peak wavelength 495 nm and 30 nm FWHM) was led to the cuvette containing the QD aqueous solution in the form of a train of pulses (pulse duration was ca 1.4 ns) at 1 MHz. The detector was set at 596 nm (QD fluorescence peak wavelength) with a bandpass of 2 nm. There were 2048 TAC channels with a variable integration time δ ranging from 50 ns to 1 μs. The photon counting was stopped when the maximal number of photon counts of the TAC channels reached a pre-set maximal

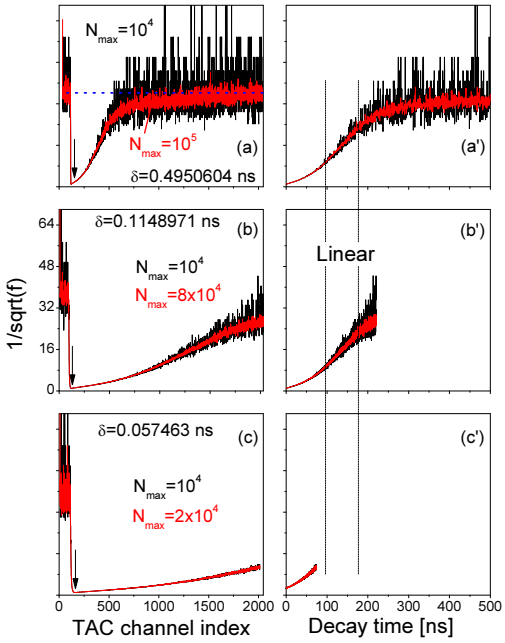

Fig. 4 (a,b,c) $\sqrt{1/f_n(\ell)}$ vs. TAC channel index ℓ as a function of $N_{\max}$ and δ. (a',b',c') $\sqrt{1/f_n(\ell\delta)}$ vs. decay time $t = \ell\delta$.

photon-count value $N_{\max}$. δ and $N_{\max}$ were adjusted in order to reach a high signal-to-noise ratio.

In order to compare the experimental decay spectrum with Eqs. (7,10), we normalized $F(\ell)$

$$f_n(\ell) = \frac{F(\ell)}{N_{\max}} \qquad (11)$$

$1/\sqrt{f_n(\ell)}$ of various $N_{\max}$ and δ are presented in Fig. 4. The dashed horizontal line in Fig. 4(a) showed that the noise levels before and long after the excitation pulse were aligned, ensuring that the QD fluorescence was excited by a single light pulse. Fig. 4(a) shows a TAC channel range from 130 (vertical arrow) to 500, corresponding to the decay time window $\in (0, 175)$ ns in Fig. 4(a'). The signal-to-noise ratio was significantly improved when $N_{\max}$ was increased.

In order to efficiently utilize the TAC channels, we decreased δ and the results are presented in Fig. 4(b) and (c). While Fig. 4(c) is commonly reported in literature, its time range is too short to unravel the linear range between the two vertical dashed lines in Figs. 4(a'), (b') and (c') that is directly correlated to the exciton radiative recombination process.

In Figs. 3 and 4, the data were recorded from a QD ensemble in aqueous solution, whereas the model of Fig. 2 applies for one exciton in a single QD. The assumption of one exciton per one QD is valid in our experimental setup since the excitation laser is too weak to excite multiple excitons. The issue of

a single QD vs. an ensemble of singe QDs needs a close examination (the QDs in solution were isolated single QDs because they were blinking under continuous excitation). The peak of the fluorescence of a QD solution is normally quite broad with a FWHM typically about 25 nm. It is generally accepted, as mentioned before, that the broad fluorescence peak of QDs in solution is due to the distribution of QD sizes. What we did in measuring the time-resolved fluorescence decay spectra here was to reduce the bandpass of the detector to only 2 nm so that we collected only the fluorescence signals from QDs of one size, if QD size distribution is the sole cause of the broad FWHM. Our experimentally measured time-resolved fluorescence decay spectra thus complied with the pre-assumptions of and therefore can be described by Eqs. (7,10).

Fig. 4 shows a clear match between the long-time time-resolved fluorescence and Eq. (10). It is thus concluded that the time-resolved fluorescence decay spectrum reflects directly and quantitatively the energy relaxation and the radiative recombination of the exciton in the QD.

3 Fluorescence spectrum of single QD

As mentioned before, we studied QD fluorescence spectrum by applying time-dependent quantum Monte Carlo simulation method that included radiative and non-radiative resonance and off-resonance transitions among confined exciton states and found that the fluorescence peak of a single QD was intrinsically broad due to resonance and off-resonance exciton radiative recombinations from time-dependent Golden rule[32,34]. To validate this theoretical result, we tried to measure the fluorescence spectra of single QDs. A drop of the QD solution was deposited into a circular area formed by nail polish on a microscope slide then covered by a coverslip. Fluorescence emissions from QDs deposited on the microscope slide were excited by a 488 nm excitation laser using a structured illumination microscope (Zeiss Elyra PS) with a 63×1.4 NA oil immersion objective (Carl Zeiss) and recorded over a bandwidth of 562–637 nm with a spectral resolution of 2.9 nm. The image frame size was 26.99×26.99 μm^2 (512×512 pixels). Software ImageJ was used to obtain the fluorescence spectra of single QDs.

Two QD samples were prepared and studied. One was quite diluted (QD concentration 10 pM) so that the optical spectra of single QDs were obtained, see Fig. 5(a). The other sample contained highly concentrated QDs which resulted in an optical spectrum of a QD ensemble, see Fig. 5(b).

The fluorescence spectra of 15 randomly chosen single QDs from the diluted sample (a) are presented in Fig. 5(c) as black solid lines, together with the optical spectrum of the QD ensemble from sample (b), indicating that the optical spectra of single QDs and the QD ensemble are very similar. Note that the fluorescence spectrum of the QD ensemble in sample (b)

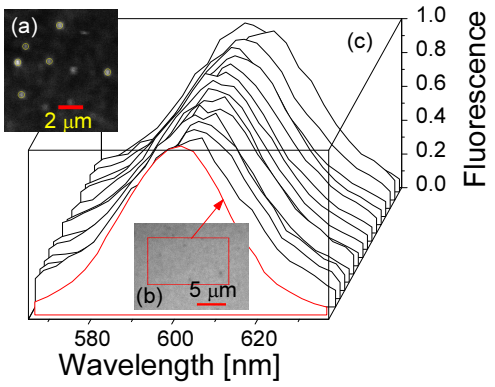

Fig. 5 (a) One image frame showing the spatial locations of single QDs in the diluted sample. (b) One image frame of the highly concentrated QDs. (c) Fluorescence spectra of single QDs (black lines) and the compact QD ensemble (red line)

was identical to the one of QDs in solution in the cuvette for the time-resolved fluorescence decay measurements. Straightforward spectral analysis showed that the FWHMs of the QD ensemble and QDs in solution were ca 33 nm, and the averaged FWHM of the 15 single QDs was also around 33 nm with individual FWHMs ranging from 32 nm to 39 nm.

We examined the spectral diffusion of our structured illumination microscope by measuring the spectrum of the excitation laser light reflected from the microscope slide. The FWHM of the reflected spectral peak was less than 5 nm (see also Ref.[42]), far narrower than the QD fluorescence peak. It was therefore safe to conclude that the large FWHM (ca 33 nm) of the single QD fluorescence peak is intrinsic.

4 Resonance and off-resonance fluorescence lifetimes

From the scattering theory and the generalized Fermi golden rule, the temporal development $\hat{T}$ of exciton state ψ_1 is described by[41,43]

$$\langle\psi_1|\hat{T}(t)|\psi_1\rangle \approx e^{-w_1 t/2} \tag{12}$$

where $1/w_1$ is the decay time of ψ_1, which is given as

$$w_1(\hbar\omega) = \frac{2\pi}{\hbar}\left|\langle\psi_0|\sum_i V_i|\psi_1\rangle\right|^2 \frac{\Gamma_1}{\Gamma_1^2+(E_1-E_0-\hbar\omega)^2} \tag{13}$$

E_1 and E_0 are energies of ψ_1 and ψ_0, respectively. $\hbar\omega$ is the photon energy. V_i is the i'th interaction between ψ_1 and ψ_0. $\Gamma_1=\hbar w_1/2$ is the relaxation energy of ψ_1 due to interactions V_i with ψ_0.

Eq. (13) implies a short resonance fluorescence lifetime (i.e., large w_1 when $E_1-E_0-\hbar\omega=0$) and a long off-resonance fluorescence lifetime. We therefore tried to find the

origin of the large FWHM of our QDs by tuning the detection wavelength of our time-resolved fluorescence decay measurement setup to scan our QD fluorescence peak with a bandpass of only 1 nm which was much smaller than the FWHM of our QDs. The measured fluorescence decay spectra $F(\ell)$ at various detection wavelengths are presented in Fig. 6(a). Here $\delta = 0.4950604$ ns while $N_{\max}$ were preset to 10^5. At off-resonance wavelengths we had to reduce $N_{\max}$ in order to obtain $F(\ell)$ within a reasonable time before the laser pulse train heated up the QDs.

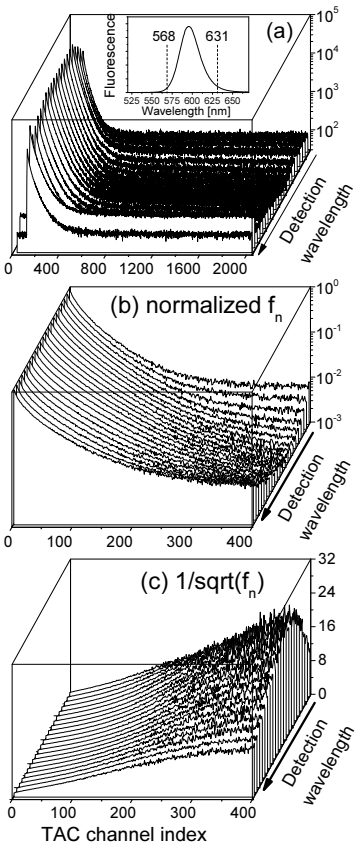

Fig. 6 (a) Time-resolved fluorescence decay spectra $F(\ell)$ of our QD solution measured at different detection wavelengths $\in (568, 631)$ nm while the detection bandpass was fixed to be 1 nm. Inset shows the fluorescence spectrum of the QD solution. (b) Normalized $f_n(\ell)$. (c) $1/\sqrt{f_n(\ell)}$. $\delta = 0.4950604$ ns

We normalized $F(\ell)$ to obtain $f_n(\ell)$ by Eq. (11), which are presented in Fig. 6(b) showing a strong detection-wavelength dependence of the fluorescence decay, especially at long decay time, which is much better visualized in $1/\sqrt{f_n(\ell)}$ in Fig. 6(c). More profoundly, the profile of the long-time $1/\sqrt{f_n(\ell)}$ vs. the detection wavelength is almost identical to the fluorescence spectrum of our QDs shown as the inset in Fig. 6(a).

Note that the measured spectrum $f_n(\ell)$ of Eq. (11) is a convolution of the time-resolved fluorescence $f(t)$ defined by Eq. (6) and the instrumental response function $p(\ell)$ of the time-correlated single-photon counting machine, i.e., the prompt signal shown in Fig. 3(a). We used software DAS6 v6.1 (decay analysis software with de-convolution) that takes the instrumental response function into account to fit $F(\ell)$ in Fig. 6(a) in a photon count range of $\in (0.9, 0.5)N_{\max}$ by a single decay term $e^{-t/\tau'}$. Since $p(\ell)$ of our system is very narrow in ℓ while the variation of $f_2(t)$ (long decay time t) in t is rather small, the effects of the numerical de-convolution of $p(\ell)$ and $F(\ell)$ at large ℓ are negligible so that we could fit directly the spectra in Fig. 6(c) by Eq. (10) to obtain β'. The resulting τ' and β' are presented in the inset of Fig. 7 (the value of β' was scaled down by a factor of 10).

Moreover, the $(0.9, 0.5)N_{\max}$ range in obtaining τ' i.e., the grey region in Fig. 2a, is determined by the time window after n_1 reaches its peak value and before n_2 decreases below n_1, within which the fluorescence decay spectrum can be well approximated by a single exponential decay.

We adjusted τ and β in Eqs. (5) so that $f(t)$ from Eq. (6) had the same τ' and β' in the inset of Fig. 7, which are presented in Fig. 7 showing that both τ and β depend strongly on the detection wavelength. Most importantly, the relationships between τ and $1/\beta$ and the detection wavelength agree well with the QD fluorescence spectrum. At QD fluorescence peak wavelength, $\tau = 8.0$ ns and $\beta = 2.0$ ns which were used in calculating Fig. 2.

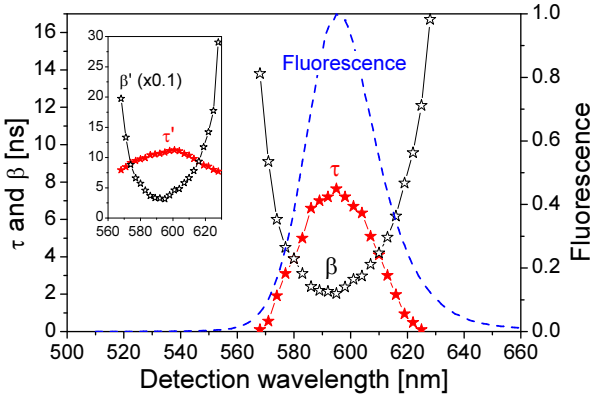

Fig. 7 Fitting parameters as functions of the detection wavelength. Solid stars: τ; hollow stars: β. Normalized QD fluorescence spectrum is presented as the dashed line for comparison. Inset shows τ' and β' (β' is scaled down by a factor of 10).

The strong dependences of τ and β on the detection wavelength and their symmetry with respect to the fluorescence peak wavelength suggest that the large FWHM of our QDs is most probably due to the resonance and off-resonance exciton radiative recombination processes, instead of being dominantly determined by the QDs' size distribution (since it is

expected physically that the changes in τ and β as functions of the QD size should be monotonic).

As shown in Fig. 1, τ describes the energy relaxation from the excited exciton state ψ_n to the ground exciton state ψ_1. The energy relaxation processes in common semiconductors are electron-phonon interactions. The energy of the most active optical phonons is $\hbar\omega_p = 37$ meV in bulk CdSe[44,45]. Similar to Eq. (13), the rate of the electron-phonon ("ep") interaction between two exciton states ψ_n and ψ_1 is proportional to

$$w_{\rm ep} = \frac{2\pi}{\hbar}|\langle\psi_1|V_{\rm ep}|\psi_n\rangle|\frac{\Gamma_p}{\Gamma_p^2+(E_n-E_1-\hbar\omega_p)^2} \qquad (14)$$

where Γ_p is the relaxation energy of the electron-phonon interaction. $w_{\rm ep}$ is maximal when $E_n - E_1 = \hbar\omega_p$. Because $\hbar\omega_p$ of semiconductor nano structures remained the same as in the bulk material[41], while the exciton states in quantum nano structures are discrete, the electron-phonon interaction rate in a semiconductor nanostructure can be very low when $E_n - E_1 \neq \hbar\omega_p$, which is known as the phonon bottleneck, see, e.g., Ref.[36,46]. Note that the electron-phonon interactions between high-energy exciton states in our QDs are not expected to be much limited due to the high density of exciton states as well as small energy separations between them[47]. We thus can expect a peak of $\tau = 1/w_{\rm ep}$ centered at E_1, as shown in Fig. 7. Moreover, the FWHM of the τ distribution peak of our QDs is about 33 nm (ca 110 meV, the same as the FWHM of the QD fluorescence peak), which is larger than $2\hbar\omega_p = 74$ meV which is expected when the electron-phonon interaction is the dominant factor in determining τ. One very possible reason for the relatively larger FWHM is that we approximated many high-energy exciton states by a single state E_n in Eq. (14).

β describes the radiative recombination of the ground exciton state ψ_1 to vacuum state ψ_0. By including only the light-matter interaction between ψ_1 and ψ_0, i.e., the radiative recombination process in Eq. (13), it was estimated that for our QDs of radius 5 nm and $E_1 - E_0 = 595$ nm, $\Gamma_1 = 0.25$ meV and $1/w_1 = \beta = 1.3$ ps at resonance ($E_1 - E_0 - \hbar\omega = 0$)[41]. It is then easy to estimate by Eq. (13) that at off-resonance of $\hbar\omega = 595 \pm 1$ nm, $\beta_{\pm 1} = 0.25$ ns. And at off-resonance of $\hbar\omega = 595 \pm 10$ nm, $\beta_{\pm 10} = 26$ ns. These numbers agreed well with β in Fig. 7. Note that $\beta = 1.3$ ps was estimated for the radiative recombination at resonance for our QDs. At off-resonance of ± 10 nm, $\beta_{\pm 10} = 26$ ns, which is four orders of magnitude longer than in the resonance situation, due to the small $\Gamma_1 = 0.25$ meV, while the energy difference between photons at wavelength 595 nm and 585 nm is 35.6 meV. In realistic measurements, the detection bandwidth is always finite so that it is very difficult to realize the perfect resonance condition. Moreover, there are nonradiative recombination processes as well as electron-phonon-interaction-assisted optical transition[48]. These two factors are most possibly the major reasons that reported radiative recombination time in CdSe QDs is in the order of nanoseconds, e.g., see Ref.[49,50].

5 Discussions

At the fluorescence peak wavelength, the extracted energy relaxation time of $\tau = 8$ ns with a detection bandpass of 2 nm, see Fig. 7, is much longer than many individual energy relaxation processes in nanometer CdSe and CdSe/ZnS heterostructures, such as the ps-order Auger-type energy relaxation process[47,51], and ps-order 1P-to-1S intraband electron relaxation obtained by measuring femtosecond transient absorption of CdSe QDs[52]. On the other hand, there have been extensive experimental works demonstrating long relaxation times in the order of ns in nanostructures, e.g., see Ref.[53,54]. Relaxation time longer than 1 ns was reported in colloidal CdSe QDs[55]. A major difference between the short and long energy relaxation processes is that the former involves limited numbers of discrete energy levels and energy relaxation processes, while the numbers of energy levels and energy relaxation processes in the latter are much higher. When multiple phonon effects were included in a perturbation calculation, a ns-order electron energy relaxation was obtained[56]. We further notice the fact that the density of exciton states in the QD increases drastically when the exciton energy becomes higher than the energy of the ground exciton state, see, e.g., Ref.[47], which is clearly reflected in the absorption spectrum of the QD that the absorption of the QD increases very quickly when the photon energy exceeds the energy of the first absorption peak. Another critical aspect about colloidal QDs is their huge superficial surfaces and a large number of surface ligands which can trap either the electron or the hole to prolong the energy relaxation processes. In other words, the representative exciton state $\hbar\omega_n$ in Fig. 1 represents a group of exciton states undergoing many energy relaxation processes and there are many exciton states between ψ_n and ψ_1.

We applied Eqs. (7) and (10) to fit our previously reported time-resolved fluorescence decay spectra[4] of QDs in the presence of free Ca^{2+} ions and EGTA (ethylene glycol tetraacetic acid, which chelates Ca^{2+}), which were analyzed by the bi-exponential model of Eq. (1). The QDs here had a fluorescence peak wavelength at 607 nm. $N_{\rm max}$ was 10000, excitation laser wavelength was 495 nm, the center of the detector wavelength at 607 nm, and the detection bandpass 2 nm. The extracted τ decreased while β increased following monotonically the increase of the Ca^{2+} concentration. They recovered when EGTA was added which chelated Ca^{2+} in the QD solution. This confirms the proposed mechanisms that the introduction of Ca^{2+} at the QD surface attracts the photogenerated electron and repels the hole, facilitating the transport of the electron and the hole between exciton states in the QD core and surface states by applying the surface-state associated blinking model, see e.g. Ref.[57]. The energy relaxation

time τ was reduced because of the increased energy relaxation channels, i.e., the number of V_i terms in Eq. (13), at the QD surface (including surface states). Furthermore, because of the increased spatial separation between the electron and the hole, $|\langle\psi_0|\sum_i V_i|\psi_1\rangle|$ in Eq. (13) is reduced, resulting in a reduced radiative recombination of the exciton and thereafter an increased β.

The effect of surface states to the fluorescence decay discussed in the above paragraph agreed with the further observation reported in Ref.[4] that at the same time τ was decreased following the Ca^{2+} concentration increase in the QD solution, the on-state probability in the single QD blinking was reduced since a Ca^{2+} ion at the QD surface increased the effect of surface states. In Ref.[1], Fisher et al. reported that in the emission-intensity trajectory, the florescence decay was long when the fluorescence intensity was high, and single-exponential fluorescence decay was observed at maximum fluorescence intensities. The experimental data can be well understood by the correlation between surface states and τ. At maximum fluorescence intensities, the effect of surface states to τ is minimal so that the energy relaxation process of an exciton from ψ_n to ψ_1 will be slow, i.e., τ is long compared with β. In this case, the fluorescence decay is dominantly determined by the single-exponential decay from ψ_n to ψ_1 since an exciton occupying ψ_1 will transit quickly to ψ_0 (short β) as compared with the exciton relaxation from ψ_n to ψ_1 (long τ). In different situations when τ is comparable with β we expect different decay characters in different time windows.

6 Summary

By narrowing the detection bandpass and increasing the signal-to-noise ratio in measuring time-resolved fluorescence decay spectrum of colloidal CdSe-CdS/ZnS QD, we have shown that directly after the photoexcitation, QD's fluorescence decay spectrum is characterized by an exponential decay due to the energy relaxation of the photogenerated exciton from its initial high-energy exciton state to the largely empty ground exciton state. At long decay time, the high-energy exciton state is basically empty, and the fluorescence is determined by the radiative recombination of the exciton from the ground exciton state to the vacuum state, both states are now partially occupied. Because of the Pauli exclusion principle, the long-time fluorescence decay spectrum is in the form of β/t^2, which is hardly exponential. Here β is the radiative recombination time of the ground-state exciton and t is the decay time. Furthermore, β is minimal at fluorescence peak wavelength suggesting that the observed broad QD fluorescence peak is most probably due to resonance and off-resonance exciton radiative recombination processes.

Colloidal quantum dots (QDs) have been the subject of extensive research and technical development. Time-resolved fluorescence decay spectrum has been widely used as an effective method to characterize QDs in various environments. Our work unravels quantitatively the link between the fluorescence decay of QDs and microscopic physical and chemical processes in the environment surrounding the QDs. We believe our work will be very useful, providing new analyses of time-resolved fluorescence spectra of QDs opening for new means for optical detection and studies of microscopic physical and chemical events.

Acknowledgement The work was supported by Swedish Research Council (621-2011-4381) and the Knut and Alice Wallenberg Foundation (KAW 2011.0218).

References

1 B. R. Fisher, H. J. Eisler, N. E. Stott and M. G. Bawendi, *J. Phys. Chem. B*, 2004, **108**, 143–148.
2 B. Mahler, P. Spinicelli, S. Buil, X. Quelin, J. P. Hermier and B. Dubertret, *Nature Materials*, 2008, **7**, 659–664.
3 O. Chen, J. Zhao, V. P. Chauhan, J. Cui, C. Wong, D. K. Harris, H. Wei, H. S. Han, D. Fukumura, R. K. Jain and M. G. Bawendi, *Nature Materials*, 2013, **12**, 445–451.
4 L. Li, Y. Chen, G. Tian, V. Akpe, H. Xu, L. M. Gan, S. Skrtic, Y. Luo, H. Brismar and Y. Fu, *J. Phys. Chem. C*, 2014, **118**, 10424–10433.
5 M. Jones, J. Nedeljkovic, R. J. Ellingson, A. J. Nozik and G. Rumbles, *J. Phys. Chem. B*, 2003, **107**, 11346–11352.
6 S. Hohng and T. Ha, *ChemPhysChem*, 2005, **6**, 956–960.
7 Y. Xing, Q. Chaudry, C. Shen, K. Y. Kong, H. E. Zhau, L. W. Chung, J. A. Petros, R. M. O'Regan, M. V. Yezhelyev, J. W. Simons, M. D. Wang and S. Nie, *Nature Protocols*, 2007, **2**, 1152–1165.
8 V. Fomenko and D. J. Nesbitt, *Nano Lett*, 2008, **8**, 287–293.
9 M. Mahmoudi, V. Serpooshan and S. Laurent, *Nanoscale*, 2011, **3**, 3007–3026.
10 H. Mattoussi, G. Palui and H. B. Na, *Adv. Drug Deliv. Rev.*, 2012, **64**, 138–166.
11 T. Ichimura, T. Jin, H. Fujita, H. Higuchi and T. M. Watanabe, *Frontiers in physiology*, 2014, **5**, 273.
12 I. Tanaka, K. Kajimoto, K. Uno, O. Ohtsuki, T. Murase, H. Asami, M. Hara and I. Kamiya, *Jpn. J. Appl. Phys.*, 2005, **44**, L249–L252.
13 G. Konstantatos, I. Howard, A. Fischer, S. Hoogland, J. Clifford, E. Klem, L. Levina and E. H. Sargent, *Nature*, 2006, **442**, 180–183.
14 Z. Ning, H. Tian, H. Qin, Q. Zhang, H. Ågren, L. Sun and Y. Fu, *J. Phys. Chem. C*, 2010, **114**, 15184–15189.
15 T. You, L. Jiang, K. L. Han and W. Q. Deng, *Nanotechnology*, 2013, **24**, 245401(6).
16 I. L. Medintz, H. Mattoussi and A. R. Clapp, *Int J Nanomedicine*, 2008, **3**, 151–167.
17 C. M. Evans, L. C. Cass, K. E. Knowles, D. B. Tice, R. P. H. Chang and E. A. Weiss, *J. Coordination Chemistry*, 2012, **65**, 2391–2414.
18 J. Y. Kim, O. Voznyy, D. Zhitomirsky and E. H. Sargent, *Adv. Mater.*, 2013, **25**, 4986–5010.
19 X. Cheng, S. B. Lowe, P. J. Reece and J. J. Gooding, *Chemical Society Reviews*, 2014, **43**, 2680–2700.
20 S. F. Wuister, C. de Mello Donega and A. Meijerink, *J Chem Phys*, 2004, **121**, 4310–4315.
21 D. Ratchford, K. Dziatkowski, T. Hartsfield, X. Li, Y. Gao and Z. Tang, *J. Appl. Physics*, 2011, **109**, 103509(6).
22 U. O. S. Seker, E. Mutlugun, P. L. Hernandez-Martinez, V. K. Sharma, V. Lesnyak, N. Gaponik, A. Eychmller and H. V. Demir, *Nanoscale*, 2013, **5**, 7034–7040.

23 D. Dorfs, T. Franzl, R. Osovsky, M. Brumer, E. Lifshitz, T. A. Klar and A. Eychmüller, *Small*, 2008, **4**, 1148–1152.

24 K. E. Knowles, E. A. McArthur and E. A. Weiss, *Acs Nano*, 2011, **5**, 2026–2035.

25 Y. C. Lin, W. C. Chou, A. S. Susha, S. V. Kershaw and A. L. Rogach, *Nanoscale*, 2013, **5**, 3400–3405.

26 E. Yaghini, F. Giuntini, I. M. Eggleston, K. Suhling, A. M. Seifalian and A. J. MacRobert, *Small*, 2013, **10**, 782–792.

27 J. L. Nadeau, L. Carlini, D. Suffern, O. Ivanova and S. E. Bradforth, *J. Phys. Chem. C*, 2012, **116**, 2728–2739.

28 J. J. Li, Y. A. Wang, W. Z. Guo, J. C. Keay, T. D. Mishima, M. B. Johnson and X. G. Peng, *J. American Chemical Society*, 2003, **125**, 12567–12575.

29 J. Muller, J. M. Lupton, A. L. Rogach, J. Feldmann, D. V. Talapin and H. Weller, *Phys. Rev. Lett.*, 2004, **93**, 167402.

30 D. E. Gomez, J. van Embden and P. Mulvaney, *Appl. Phys. Lett.*, 2006, **88**, 154106.

31 D. Pal, V. G. Stoleru, E. Towe and D. Firsov, *Jpn. J. Appl. Phys.*, 2002, **41**, 482–489.

32 Y. Fu, T. T. Han, H. Ågren, L. Lin, P. Chen, Y. Liu, G. Q. Tang, J. Wu, Y. Yue and D. Dai, *Appl. Phys. Lett.*, 2007, **90**, 173102(3).

33 L. Li, G. Tian, Y. Luo, H. Brismar and Y. Fu, *J. Phys. Chem. C*, 2013, **117**, 4844–4851.

34 T. T. Han, Y. Fu and H. Ågren, *J. Appl. Phys.*, 2007, **101**, 063712(6).

35 Z. J. Ning, M. Molnár, Y. Chen, P. Friberg, L. M. Gan, H. Ågren and Y. Fu, *Phys. Chem. Chem. Phys.*, 2011, **13**, 5848–5854.

36 R. Heitz, H. Born, F. Guffarth, O. Stier, A. Schliwa, A. Hoffmann and D. Bimberg, *Phys. Rev. B*, 2001, **64**, 241305(4).

37 Y. Fu, S. Hellström and H. Ågren, *J. Nonlinear Optical Physics & Materials*, 2009, **18**, 195–226.

38 Y. Fu, *J. Appl. Phys.*, 2009, **106**, 054302(5).

39 S. H. Chang and A. Taflove, *Optics Express*, 2004, **12**, 3827–3833.

40 Y. Huang and S. T. Ho, *Optics Express*, 2006, **14**, 3575–3587.

41 Y. Fu, H. Ågren, J. M. Kowalewski, H. Brismar, J. Wu, Y. Yue, N. Dai and L. Thylén, *EuroPhysics Lett.*, 2009, **86**, 37003(6).

42 H. Xu, L. Li, O. Manneberg, A. Russom, K. B. Gylfason, H. Brismar and Y. Fu, *J. Physical Chemistry B*, 2013, **117**, 14151–14156.

43 L. D. Landau and E. M. Lifshitz, *Quantum Mechanics*, Pergamon Press, Oxford, 2nd edn, 1965.

44 D. C. Reynolds, C. W. Litton and T. C. Collins, *Phys. Rev. B*, 1971, **4**, 1868–1872.

45 A. L. Pan, R. B. Liu and B. S. Zou, *Appl. Phys. Lett.*, 2006, **88**, 173102(3).

46 J. Urayama, T. B. Norris, J. Singh and P. Bhattacharya, *Phys. Rev. Lett.*, 2001, **86**, 4930(4).

47 Y. Fu, Y. H. Zhou, H. Su, F. Y. C. Boey and H. Ågren, *J. Physical Chemistry C*, 2010, **114**, 3743–3747.

48 Z. H. Chen, S. Hellström, Z. J. Ning, Z. Y. Yu and Y. Fu, *J. Physical Chemistry C*, 2011, **115**, 5286–5293.

49 C. de Mello Donegá, M. Bode and A. Meijerink, *Phys. Rev. B*, 2006, **74**, 085320(9).

50 M. Califano, A. Franceschetti and A. Zunger, *Phys. Rev. B*, 2007, **75**, 115401(7).

51 A. L. Efros, V. A. Kharchenko and M. Rosen, *Solid State Commun.*, 1995, **93**, 281–284.

52 V. I. Klimov and D. W. McBranch, *Phys. Rev. B*, 1999, **60**, 13740–13749.

53 K. Mukai, N. Ohtsuka, H. Shoji and M. Sugawara, *Appl. Phys. Lett.*, 1996, **68**, 3013–3015.

54 A. J. Nozik, *Ann. Rev. Phys. Chem.*, 2001, **52**, 193–231.

55 A. Pandey and P. Guyot-Sionnest, *Science*, 2008, **322**, 929–932.

56 T. Inoshita and H. Sakakia, *Physica B*, 1996, **227**, 373–377.

57 P. Frantsuzov, M. Kuno, B. Janko and R. A. Marcus, *Nature Physics*, 2008, **4**, 519–522.